Sonolytic Decomposition of Aqueous Bioxalate in the Presence of Ozone

Chad D. Vecitis, Timothy Lesko, Agustin J. Colussi, and Michael R. Hoffmann*

W.M. Keck Laboratories, California Institute of Technology, Pasadena, California 91125

Received: December 4, 2009

Ultrasonic irradiation in the presence of ozone is demonstrated to be effective for the rapid oxidation of oxalic acid, bioxalate, and oxalate ($H_2C_2O_4/HC_2O_4^-/C_2O_4^{2-}$) in aqueous solution to CO_2 and H_2O. The degradation rate of bioxalate exposed to "sonozone" (i.e., simultaneous ultrasonication and ozonolysis) was found to be 16-times faster than predicted by the linear addition of ozonolysis and ultrasonic irradiation rates. The hydroxyl radical ($^{\bullet}OH$) is the only oxy-radical produced that can oxidize oxalate on a relevant timescale. Thus, plausible $^{\bullet}OH$ production mechanisms are evaluated to explain the observed kinetic synergism of ultrasonication and ozonolysis toward bioxalate decomposition. $^{\bullet}OH$ production via decomposition of O_3 in the cavitating bubble vapor and via the reaction of O_3 and H_2O_2 are considered, but kinetic estimations and experimental evidence indicate neither to be a sufficient source of $^{\bullet}OH$. A free-radical chain mechanism is proposed in which the $HC_2O_4^- + {}^{\bullet}OH$ reaction functions as a primary propagation step, while the termination occurs through the $O_3 + CO_2^{\bullet-}$ reaction via an O-atom transfer mechanism. Kinetic simulations confirm that ozone reacts efficiently with the superoxide ($O_2^{\bullet-}$) ion that is produced by the reaction of O_2 and $CO_2^{\bullet-}$ to form $^{\bullet}OH$ radical, and that the reaction of $O_3 + CO_2^{\bullet-}$ must be chain terminating. Oxalate is also readily oxidized by "peroxone" treatment (i.e., H_2O_2 and O_3). However, the addition of H_2O_2 during the course of the sonolytic ozonation of oxalic acid does not appear to increase the observed degradation rate and decreases rates at millimolar levels.

Introduction

Oxalic acid is a common phytochemical that is also produced during incomplete biomass burning,[1] during the photodegradation of humic substances and natural organic matter (NOM),[2,3] and via the ring-opening oxidation of aromatic compounds.[4−9] As a consequence, oxalate ["oxalate" ≡ $H_2C_2O_4$ (oxalic acid) + $HC_2O_4^-$ (bioxalate) + $C_2O_4^{2-}$ (oxalate)] is routinely detected in terrestrial and aquatic environments as well as in ambient aerosols.[1,2,10] Oxalate is moderately recalcitrant toward oxidation, and it often accumulates in natural waters where it can lead to microbial growth.[2,11,12] Exposure to high oxalate concentrations has detrimental health effects such as kidney and renal cell damage, nutrient deficiencies, and lithiasis.[13−16] Therefore, any advanced water or wastewater process should include provisions for the complete degradation of oxalates.

The chemistry of aqueous oxalate degradation has been investigated for more than 50 years. Oxalate has been eliminated from water by oxidation as catalyzed by various transition metals,[17,18] by permanganate,[19] peroxydisulfate,[20] bromine,[21] and by metal oxide photocatalysis.[22] Several studies were focused on the use of several metal-ion catalysts combined with ozone to enhance the degradation of oxalate in aqueous solution.[23−27] Oxalic acid is fairly resistant to oxidation with ozone alone; however, in the presence of some metal ion catalysts, oxalate can be converted to CO_2 during ozonolysis. The increased extent of oxidation of oxalate in the metal-catalyzed ozone reaction is achieved via a mechanism in which ozone effectively recycles the higher oxidation states of metal ions, which in turn oxidize the metal complexed oxalate.[24,26]

While $H_2C_2O_4$, $HC_2O_4^-$, and $C_2O_4^{2-}$ are known scavengers of e_{aq}^- and $^{\bullet}OH$,[28−30] previous investigations have indicated that $^{\bullet}OH$-mediated degradation of oxalate by high frequency ultrasound results in minimal degradation.[31,32] In an attempt to improve the efficiency of the sonolytic oxidation of oxalate, we examined the combination of ultrasonic irradiation with ozonolysis. Using the coupled techniques, we found that oxalate degradation rates significantly exceeded the addition of the independent rates for ozone and oxalate and for ultrasound and oxalate. While previous investigations found that the combination of ozone and ultrasonic irradiation to be effective at enhancing the degradation and mineralization of various organic solutes in aqueous solution,[6,33−35] the synergism observed in our system appears to be unique.

The principal objective of this study is to investigate the mechanism of the strong synergistic effect of sonolysis combined with ozonolysis for the oxidation of oxalic acid. The degradation pathways of the individual oxidation techniques are discussed and several degradation mechanisms are considered that may account for the observed rate enhancements when the two systems are combined.

Experimental Methods

Experiments were performed in a 605 mL bench-scale sonochemical reactor (Allied Signal-ELAC Nautik USW). The ELAC reactor employs a bottom-mounted 358 kHz transducer operated between 0 and 100 W. The reactor is a glass vessel with an integrated water jacket for cooling. Aqueous samples were chilled to 15 °C with a 1.5 kW thermostat (VWR 1157). The vessel is sealed with a hemispherical glass top with several sampling ports. One of the ports was left open to the atmosphere to allow for gas exchange. The emitting area of the ELAC transducer is 23.6 cm^2. The reported applied power for the small reactors has been previously determined using standard calorimetric procedures.[36]

* To whom correspondence should be addressed. E-mail: mrh@caltech.edu. Telephone: +1-626-395-4391.

10.1021/jp9115386
Published on Web 03/15/2010

TABLE 1: Carbon Dioxide Radical Reactions and Rate Constants Added to FACSIMILE Model

eq No.	chemical reaction	k (M^{-1} s^{-1})	reference
	$US \rightarrow HO^{\bullet}_{(bulk,aq)}$	1.4×10^{-8}	this work
12/13/14	$HC_2O_4^- + OH \rightarrow CO_2^{\bullet-} + CO_2 + H_2O$	3.2×10^7	Buxton et al.[40]
16	$CO_2^{\bullet-} + CO_2^{\bullet-} \rightarrow C_2O_4^{2-}$	5.0×10^8	Ross et al.[41]
17	$CO_2^{\bullet-} + O_2 \rightarrow CO_2 + O_2^{\bullet-}$	2.0×10^9	Ross et al.[41]
40a	$CO_2^{\bullet-} + O_3 \rightarrow CO_2 + O_3^{\bullet-}$	0	this work
40b	$CO_2^{\bullet-} + O_3 \rightarrow CO_3^{2-} + O_2$	$1.5 \pm 0.5 \times 10^8$	this work

Ozone was generated with a corona discharge ozone generator (Orec V10−0). The O_2 feed gas was dried and purified with a molecular sieve and Drierite cartridge (Alltech) prior to entering the instrument. The O_2/O_3 mixture was delivered to a solution in the reactor via a medium porosity glass frit and was sparged during sonication. Varying the voltage and flow rates of the of the ozone generator regulated ozone concentrations. Gas flow rates were monitored with a gas flow meter (Gilmont Instruments). Steady state concentrations of ozone in the small reactor ranged from 0 to 400 μM.

Aliquots were sampled with a glass syringe that was fitted with a stainless steel needle and were stored in amber glass vials and then analyzed to quantify the concentration of the substrates. Anion concentrations were quantified using a Dionex Bio LC ion chromatograph. Separations were carried out on a 25 cm AS11 column with a 0.01−0.1 M NaOH eluent with a flow rate of 2 mL/min. Total organic carbon concentrations were measured with a Shimadzu TOC 5000 A organic carbon analyzer with a Shimadzu ASI 5000A autosampler. A heated course catalyst bed was heated to 680 °C. Samples were acidified with HCl to pH 1−2 and purged for 1 min prior to injection with instrument grade air to remove any dissolved carbonate or bicarbonate. Samples were analyzed in triplicate.

Aqueous ozone concentrations were determined in a 1 cm path length quartz cuvette with a Hewlett-Packard 8452 A diode-array spectrophotometer at $\lambda = 260$ nm ($\varepsilon_{aq,O_3} = 3292$ M^{-1} cm^{-1}). Ozone concentrations were monitored indirectly with iodometry in solutions containing oxalate due to absorption interferences at 260 nm. Sample aliquots were added to flasks containing KI (1% w/w, 0.06 M) in a phosphate solution at pH 7, the absorbance of I_3^- ($I^- + I_2 \rightarrow I_3^-$) was monitored at $\lambda =$ 350 nm, and a set of calibrations were performed to demonstrate the direct correlation with ozone concentrations.

H_2O_2 solutions were prepared by dilution of 30% H_2O_2 (EM Science) in purified H_2O. Concentrations were quantified by UV-spectroscopy at $\lambda = 248$ nm ($\varepsilon_{H_2O_2} = 25$ M^{-1} cm^{-1}), or by iodometry using ammonium molybdate (0.02% w/w, 1.1 mM) as a catalyst.[37] pH measurements were made with a Beckman Altex 71 pH meter and a Beckman glass pH electrode (model 39843).

The kinetics of oxalate degradation were determined under constant levels of ozonolysis and ultrasonic irradiation. The O_3 steady-state concentrations for these experiments were determined before the addition of $H_2C_2O_4$ or the imposition of the acoustic field. To ensure that $[O_3]_{ss}$ remained constant during the course of an experiment, a separate vessel containing ultrapure H_2O was sparged with the same ozone stream and the $[O_3]$ was determined. The maximum variation in $[O_3]_{ss}$ during the experiment was ± 10 μM.

Separate experiments were performed to investigate the decomposition kinetics of ozone in the presence of ultrasound and/or oxalate. Ultrapure water was sparged with O_2/O_3 for an hour until $[O_3]_{aq}$ reached ~100 μM. To initiate a reaction, oxalate solutions were added into the O_3 solution. At this point, the flow of O_2/O_3 gas supply was interrupted, and $[O_3]$ at $t =$ 0 was determined.

Oxalic acid ($H_2C_2O_4$) (Baker, >99.5%), KI (Sigma, ≥99.0), NaH_2PO_4 (Mallinckrodt, ≥99.0), Na_2HPO_4 (Mallinckrodt, ≥99.0), $NaCO_2H$ (Mallinckrodt, ≥99.0), $NaC_2H_3O_2$ (Mallinckrodt, ≥99.0), $(NH_4)_6Mo_7O_{24}\cdot 4H_2O$ (Alfa Products), and H_2O_2 (EM Science, 30%wt) were used without further purification. Water used for sample preparation was purified with a Millipore Milli-Q UV Plus system ($R = 18.2$ MΩ cm^{-1}). All pH measurements were made with a Beckman Altex 71 pH meter. The reaction kinetics were measured in unbuffered systems.

The experimental bioxalate ($HC_2O_4^-$) and ozone decay profiles were simulated by numerical integration of the reaction mechanisms based on the set of elementary reactions given in Table 1 using the FACSIMILE equation solver.[38] Reaction rate constants were obtained from literature compilations.[39−41] During simultaneous ozonolysis and sonolysis, the aqueous-phase ozone, oxygen, and carbon dioxide concentrations were assumed to be constant. Aqueous-phase or dissolved-phase ozone was determined experimentally and the dissolved oxygen was calculated from the Henry's Law relationship to be 0.33 mM without ozone and 1.5 mM with ozone. Ultrasound was considered to be a blackbox source of aqueous hydroxyl radical from which the production hydroxyl radical generation rate was estimated based on the work of Hua and Hoffmann.[42]

The rate constant for the reaction of hydroxyl radical and the carbon dioxide radical to from bicarbonate was assumed to be diffusion limited for which the second-order rate constant was assume to be $k \approx 1 \times 10^{10}$ $M^{-1}s^{-1}$ since hydroxyl radical ($E^0 = 1.9$ V) is a strong one-electron oxidant, and the carbon dioxide radical ($E^0 = -1.9$ V) is an equally strong one-electron reductant. This reaction is not expected to affect the rate of disappearance of the carboxyl radical, since its main reaction pathway is with dissolved oxygen or ozone (i.e., $k = 2 \times 10^9$ and $[O_2]_{aq} \approx 0.0012$ M). Even at diffusion-limited rates, the hydroxyl radical concentration would need to be $[OH]_{ss} > 10^{-4}$ M to compete with oxygen, which is 9 orders of magnitude higher than the steady-state hydroxyl radical concentration, $[OH]_{ss} \sim 10^{-13}$, calculated for this dynamic reaction system. In addition, the kinetics and mechanism of the reaction of ozone with the carbon dioxide radical are unknown. Either a direct electron transfer or O-atom transfer mechanism may be operative. In this case, kinetic modeling and FACSIMILE simulations were utilized to determine the most probable mechanism with a corresponding estimated reaction rate constant.

Results and Discussion

Oxalic Acid Speciation. The experiments were performed by adding $H_2C_2O_4$ to Milli-Q water to achieve a concentration

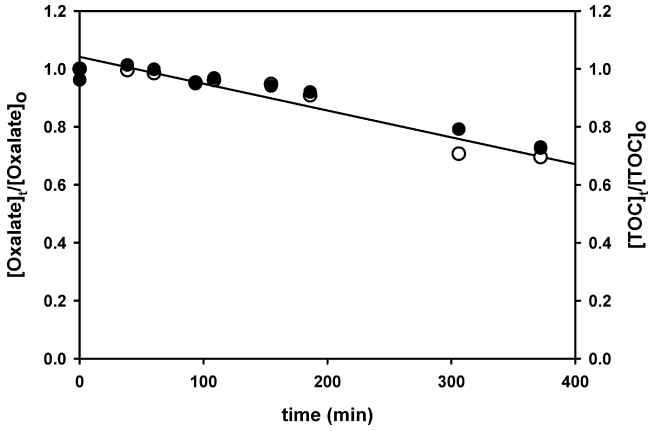

Figure 1. Degradation of $[H_2C_2O_4]_t$ with ultrasound ($[H_2C_2O_4]_0 = 0.9$ mM, 358 kHz, 100 W, 0.605 L, 15 °C, pH ~ 3). ○: normalized oxalate concentrations; ●: normalized TOC concentrations.

of 0.9 mM. The addition of oxalic acid to resulted in a pH depression from 5 to 3. The acid dissociation constants for $H_2C_2O_4$ are $pK_{a1} = 1.2$ and $pK_{a2} = 4.2$.[43] At pH 3, all three forms of oxalate may be present in solution. The fraction of each species is given by

$$\alpha_{H_2C_2O_4} = \frac{[H_2C_2O_4]}{[H_2C_2O_4]_T},\ \alpha_{HC_2O_4^-} = \frac{[HC_2O_4^-]}{[H_2C_2O_4]_T},\ \alpha_{C_2O_4^{2-}} = \frac{[C_2O_4^{2-}]}{[H_2C_2O_4]_T} \quad (1)$$

where

$$[H_2C_2O_4]_T = [H_2C_2O_4] + [HC_2O_4^-] + [C_2O_4^{2-}] \quad (2)$$

$$\alpha_{H_2C_2O_4} = \frac{[H_3O^+]^2}{[H_3O^+]^2 + K_{a1}[H_3O^+] + K_{a1}K_{a2}} \quad (3)$$

$$\alpha_{HC_2O_4^-} = \frac{K_{a1}[H_3O^+]}{[H_3O^+]^2 + K_{a1}[H_3O^+] + K_{a1}K_{a2}} \quad (4)$$

$$\alpha_{C_2O_4^-} = \frac{K_{a1}K_{a2}}{[H_3O^+]^2 + K_{a1}[H_3O^+] + K_{a1}K_{a2}} \quad (5)$$

From eqs 1−5 at pH 3, we estimate that 93% of the total oxalic acid is present in the singly protonated bioxalate species, $HC_2O_4^-$, and 6% as doubly deprotonated oxalate species, $C_2O_4^{2-}$. For comparison, at pH 5, we estimate 13% of the total oxalic acid is present in the singly protonated bioxalate species, $HC_2O_4^-$, and 6% as doubly deprotonated oxalate species, $C_2O_4^{2-}$.

Experimental $HC_2O_4^-$ Degradation Kinetics: Ultrasound, O_3, and Sonozone (US/O_3). The degradation of oxalate in aqueous solution was monitored by ion chromatography during ultrasonic irradiation ($f = 358$ kHz, $P_{app} = 100$ W, $V = 0.6$ L, $T = 15$ °C) and/or continuous ozonolysis (2.75% v/v O_3/O_2). $HC_2O_4^-$ was oxidized with apparent zero-order reaction kinetics (eq 6) for all three systems as shown in Figures 1 and 2.

$$-\left(\frac{d[oxalate]}{dt}\right) = R_{-ox} = k_{-ox} \quad (6)$$

To determine the normalized zero-order rate constant in min^{-1}, profiles of normalized solute concentrations versus time were linearly fit (eq 7) to determine the normalized zero-order rate constant, $k'_{-ox} = k_{-ox}/[H_2C_2O_4]_0$.

$$\frac{[H_2C_2O_4]}{[H_2C_2O_4]_0} = 1 - \left(\frac{k_{-ox}}{[H_2C_2O_4]_0}\right)t = 1 - k'_{-ox}t \quad (7)$$

The overall bioxalate oxidation to CO_2 and H_2O follows the stoichiometry in eq 8.

$$2HC_2O_4^- + O_2 + 2H^+ \rightarrow 4CO_2 + 2H_2O \quad (8)$$

During the course of the experiments, the reacting solutions remained clear and colorless and no additional products were observed using standard chromatographic techniques. The extent of $HC_2O_4^-$ oxidation was independently monitored by measuring the total organic carbon concentration (TOC) remaining in solution. In all cases, the TOC loss rates, $R_{-TOC} = -d[TOC]dt$, also followed zero-order kinetics. Rate constants for $HC_2O_4^-$ oxidation and TOC loss, k'_{-ox} and k'_{-TOC}, respectively, were essentially identical, indicating that the oxidation of $HC_2O_4^-$ resulted in conversion to CO_2 (i.e., no free radical polymerization to produce higher molecular weight compounds were observed).

The maximum observed rate of bioxalate oxidation via ultrasonic irradiation (358 kHz, 100 W, $[H_2C_2O_4]_0 = 0.9$ mM, and pH = 3) alone had a zero-order degradation rate of ${}^{US}R_{-ox} = 8.3 \times 10^{-7}$ M min^{-1}, Figure 1. For comparison in Figure 2, the maximum rate of $HC_2O_4^-$ oxidation by ozonolysis alone was ${}^{O_3}R_{-ox} = 9.6 \times 10^{-7}$ M min^{-1} ($[O_3]_{ss} = 340$ μM, $[H_2C_2O_4]_o = 0.9$ mM, and pH = 3). The plots were made in separate figures due to the overlap of time-dependent data. In contrast to the slow oxidation kinetics achieved with ultrasound or ozone individually, the simultaneous application of ozone and ultrasound significantly (>10×) enhanced the oxidation rate of $HC_2O_4^-$. A zero-order degradation rate of ${}^{US/O_3}R_{-ox} = 2.8 \times 10^{-5}$ M min^{-1} was obtained under ultrasonic and ozone

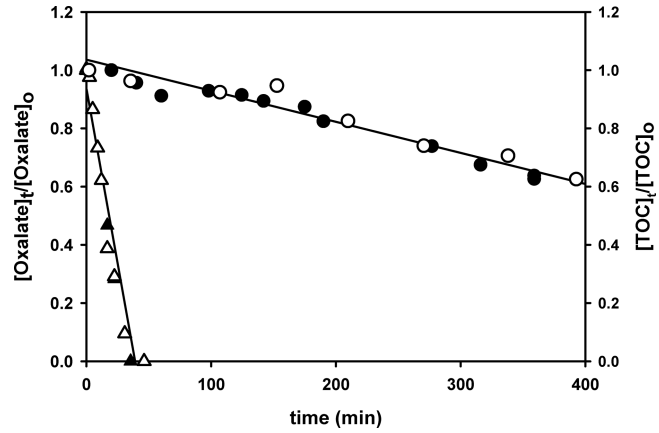

Figure 2. Degradation of $[H_2C_2O_4]_t$ with ozone and ozone/ultrasound ($[H_2C_2O_4]_0 = 0.9$ mM, 0.605 L, 15 °C, pH ~ 3). ○: normalized oxalate concentrations using ozone only ($[O_3]_{ss} = 340$ μM); ●: normalized TOC concentrations using ozone only ($[O_3]_{ss} = 340$ μM); Δ: normalized oxalate concentrations using ozone with ultrasound ($[O_3]_{ss} = 350$ μM, 358 kHz, 100 W); ▲: normalized TOC concentrations using ozone with ultrasound ($[O_3]_{ss} = 350$ μM, 358 kHz, 100 W).

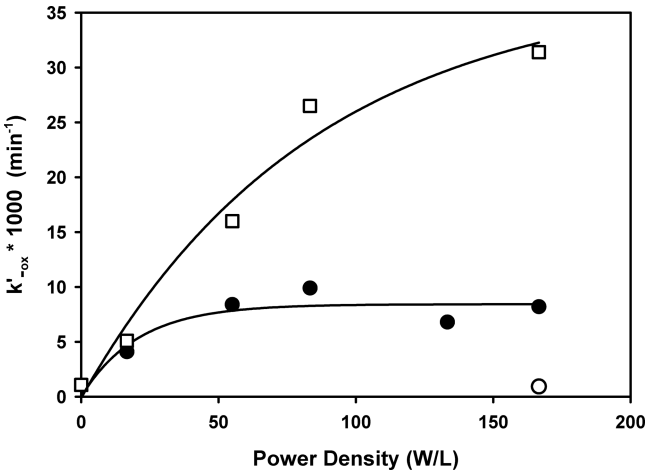

Figure 3. Normalized pseudozero-order degradation rate constants of $[H_2C_2O_4]_t$ vs ultrasonic power desity (358 kHz, 0.605 L, $[C_2H_4O_4]_0$ = 0.9 mM, 0.605 L, 15 °C, pH ~ 3). □: $[O_3]_{ss}$ =350 μM; ●: $[O_3]_{ss}$ =150 μM; ○: $[O_3]_{ss}$ = 0 μM.

conditions of 358 kHz, 100 W, $[O_3]_{ss}$ = 350 μM, $[H_2C_2O_4]_o$ = 0.9 mM, and pH = 3, see Figure 2. The combined system resulted in complete (>99%) degradation of oxalate, and loss of any quantifiable organic carbon (i.e., TOC) under 1 h of treatment. The synergistic action of the combination of O_3 and ultrasound enhanced the apparent oxalate oxidation rates 16× as compared to a simple linear addition of the two independent reaction systems.

$HC_2O_4^-$ oxidation rates were measured in the sonozone (ultrasound + O_3) system at two separate ozone concentrations, 150 and 350 μM, as a function of the applied ultrasonic power density (PD) at 358 kHz. (Figure 3) At the lower ozone concentration, a maximum rate constant of $^{US/O_3}R_{-ox} = 6.75 \times 10^{-6}$ M min^{-1} was obtained at 83 W/L. Subsequent increases in power density to 133 and to 167 W/L did not result in further increase in rate. The zero-order degradation rates at the higher ozone concentrations (350 μM) increased linearly with increasing applied power density (PD) from 0 to 83 W/L following eq 9.

$$^{US/03}R_{-ox} = 2.8 \times 10^{-7}[PD(WL^{-1})] + 2.2 \times 10^{-7} \quad (9)$$

Increasing the power density to 166 W/L increased the sonolytic degradation rates, but not to the extent as predicted from eq 9. The rate of bioxalate oxidation reaching a maximum value as a function of an increasing $[O_3]$ suggests that sonolytic ozone decomposition[44] and mass transfer out of solution eventually negates any rate enhancements from the US/O_3 combined sonozone process.

$HC_2O_4^-$ Oxidation Mechanism during Ultrasonic Irradiation. Ultrasonic irradiation of aqueous solutions results in the formation and quasi-adiabatic collapse of vapor bubbles formed from pre-existing bubble nuclei. The transient collapse of cavitation bubbles raises the internal vapor temperatures near 4000−5000 K.[45−48] The thermal decomposition of water vapor during acoustic cavitation leads to the formation of $^{\bullet}$OH, O-atom, and H$^{\bullet}$ as shown in eqs 10 and 11.

$$H_2O \xrightarrow{)))\Delta} {}^{\bullet}OH + H^{\bullet} \quad (10)$$

$$OH \xrightarrow{)))\Delta} O + H \quad (11)$$

Subsequent high temperature radical reactions produce other oxidizing species such as the hydroperoxyl radical, $HO_2^{\bullet}$, and superoxide, $O_2^{\bullet-}$. These transient radicals react readily with compounds in the gas-phase or at the bubble interface. Most of the radical species will recombine in the gas-phase or near the bubble interface to produce H_2O, O_2, and H_2O_2,[40,42,49−51] therefore only a small fraction of the radical species are dispersed throughout the bulk solution. Highly soluble ionic species such as $HC_2O_4^-$ will react primarily with the radical species that are dispersed into bulk solution during bubble collapse, consistent with slow sonochemical oxalate degradation rates.

Getoff et al.[30] investigated the reaction between $HC_2O_4^-$ and $^{\bullet}$OH using pulse-radiolysis in N_2O-saturated oxalate solutions. Their results suggest that the reaction occurs via direct electron transfer from oxalate to hydroxyl radical to form water (eq 12). However, at low pH $^{\bullet}$OH also reacts via H-atom abstraction to form water.

$$HC_2O_4^- + OH \rightarrow HC_2O_4^{\bullet}/C_2O_4^{\bullet-} + {}^-OH/H_2O \quad (12)$$

The bioxalate radical and oxalate radical anion then undergo unimolecular decompositions to yield CO_2 and the formyl/carboxyl radical, $HCO_2^{\bullet-}/CO_2^-$ according to eq 13.[28]

$$HC_2O_4^{\bullet}/C_2O_4^{\bullet-} \rightarrow {}^{\bullet}CO_2H/CO_2^{\bullet-} + CO_2 \quad (13)$$

The pK_a of the carboxyl radical is still uncertain. Measurements[52−54] have placed an upper limit of 4 on pK_a ($HCO_2^{\bullet}$) and a lower limit of −0.2.[55] Von Sonntag and co-workers[52] reported an approximate value of 2.3 as shown in eq 14. Under the pH conditions of the sonolytic oxalate system, the deprotonated $CO_2^{\bullet-}$ will be the predominant species.

$$^{\bullet}CO_2H \leftrightarrow H^+ + CO_2^{\bullet-} (pK_a \approx 2.3) \quad (14)$$

$CO_2^{\bullet-}$ is a strong, one-electron reductant, $E^0 = -1.85$ V,[56] eq 15, and will react with easily reduced organics and oxidizing radicals at diffusion-controlled rates.

$$CO_2 + e^- \rightarrow CO_2^{\bullet-} (E^0 = -1.85 \text{ V}) \quad (15)$$

In anoxic solutions, the recombination of the carboxyl anion radical in aqueous solution is known to regenerate oxalate, eq 16.[52,57]

$$CO_2^{\bullet-} \rightarrow C_2O_4^{2-} \quad (16)$$

In the presence of oxygen, $^{\bullet}CO_2H$ and $CO_2^{\bullet-}$ are scavenged by direct electron transfer to O_2 at diffusion-controlled rates, eq 17.[57]

$$^{\bullet}CO_2H/CO_2^{\bullet-} + O_2 \rightarrow HO_2^{\bullet}/O_2^{\bullet-} + CO_2 \quad (17)$$

With the pK_a for $HO_2^\bullet$ of 4.8,[58] $O_2^{\bullet-}$ will be 48.8% protonated at pH 5 and 98.5% protonated at pH 3, eq 18. The hydroxyl/superoxide species will self-react to produce hydrogen peroxide and oxygen as radical chain termination steps, eqs 19 and 20.

$$H^+ + {}^\bullet O_2^- \leftrightarrow HO_2^\bullet \quad (18)$$

$$HO_2^\bullet + HO_2^\bullet \rightarrow H_2O_2 + O_2 \quad (19)$$

$$HO_2^\bullet + O_2^{\bullet-} \rightarrow HO_2^- + O_2 \quad (20)$$

The bimolecular rate constant of eq 20 ($\sim 10^8$ M^{-1} s^{-1}) is nearly 2 orders of magnitude greater than that eq 19 ($\sim 10^6$ M^{-1} s^{-1}); thus, recombination will be accelerated at pH 5 as compared to pH 3. Upon increasing the pH further (>5) the self-reaction rate will significantly decrease since the rate of $O_2^{\bullet-} + O_2^{\bullet-}$ is negligible in comparison to eqs 19 and 20.

The second-order rate constant for the reaction of the hydroxyl radical with the three oxalic acid species has been measured by pulse radiolysis.[30] Bioxalate has the fastest reaction with $^\bullet OH$, eq 21; thus, this reaction rate will be utilized in the kinetic simulations.

$$k[{}^\bullet OH + (H_2C_2O_4/HC_2O_4^-/C_2O_4^{2-})] = 1.1 \times 10^6/3.2 \times 10^7/5.3 \times 10^6\ M^{-1}\ s^{-1} \quad (21)$$

$HC_2O_4^-$ reacts very slowly with $^\bullet O_2^-$ ($k < 0.2$ M^{-1} s^{-1}),[59] and similar rates are expected for reactions with $HO_2^\bullet$ and H_2O_2. Therefore, in the presence of ultrasound, the degradation of oxalic acid is predominantly via $^\bullet OH$ oxidation, eq 22.

$$-\left(\frac{d[H_2C_2O_4]_t}{dt}\right) \approx R_{(^\bullet OH/HC_2O_4^-)} = k[{}^\bullet OH][HC_2O_4^-] \quad (22)$$

The sonolytic decomposition of many organic compounds in water follows pseudofirst-order kinetics due to competition for $^\bullet OH$ between the initial organic and its oxidation intermediates.[6,60−62] However, as shown in Figure 1, oxalate degradation kinetics are zero-order over the course of the reaction (i.e., $[HC_2O_4^-]_t/[HC_2O_4^-]_i$ vs time is linear). This is consistent with $^\bullet OH/O_2$ oxidation of $HC_2O_4^-$ to $2CO_2$ via eqs 12, 13, and 17. At low pH, CO_2 should be rapidly sparged out of solution, thus reducing the number of reaction intermediates that may compete with bioxalate for hydroxyl radicals. The observed zero-order kinetics indicates $^\bullet OH$ is the primary oxidant and that its cavitation-dependent production rate limits the overall rate of $HC_2O_4^-$ degradation.

To confirm $^\bullet OH$, we will compare oxalate degradation rates observed here to previously estimated sonochemical $^\bullet OH$ production rates. Hua and Hoffmann[42] measured the $^\bullet OH$ production rate in water in an ultrasonic reactor operating at 513 kHz. At 39 W of applied power, they determined an $^\bullet OH_{(aq)}$ production rate of $\sim 5 \times 10^{-9}$ M s^{-1}. Assuming $^\bullet OH$ production scales linearly with applied power density and only a minor frequency dependence, at 100 W and 358 kHz, a $^\bullet OH$ production rate of 1.3×10^{-8} M s^{-1} is estimated for reactor system described in the experimental details above. This value is consistent with the observed bioxalate degradation rate of $^{US}k_{-ox} = 1.4 \times 10^{-8}$ M s^{-1}, indicating $^\bullet OH$ as the primary oxidant. The fast $^\bullet OH$ oxidation kinetics will yield low steady-state $^\bullet OH$ concentrations, eq 23.

$$^{US}R_{-ox} = {}^{US}k_{-ox} = k[{}^\bullet OH]_{ss}[HC_2O_4^-]_{ss} \quad (23)$$

Assuming steady-state conditions as given in eq 23, that $HC_2O_4^-$ is the dominant species or $k = 3.2 \times 10^7$ M^{-1} s^{-1}, and using the average oxalate concentration over the course of the reaction, $[HC_2O_4^-]_{ss} = 8.1 \times 10^{-4}$ M. A steady-state hydroxyl radical concentration of 5.4×10^{-13} M is estimated for ultrasonic irradiation of near millimolar oxalate solutions.

$HC_2O_4^-$ Oxidation Mechanism during Ozonolysis. The simplest reaction mechanism for the ozonation of bioxalate, $HC_2O_4^-$, will be via a one-electron transfer process similar to hydroxyl radical oxidation. However, due to ozone's relatively low one-electron reduction potential, the direct ozonation of bioxalate is likely not the primary decomposition mechanism as will be detailed in the following text. The half-reactions for direct one-electron ozone oxidation of bioxalate are presented in eqs 24 and 25.

$$O_3 + e^- \rightarrow O_3^{\bullet-} \quad (24)$$

$$HC_2O_4^- \rightarrow HO(O)C{-}C(O)O^\bullet + e^- \quad (25)$$

The reduction potential for the O_3/O_3^- couple is 1.02 V.[63] We have estimated the reduction potential for half-reaction found in eq 25 to be -2.0 ± 0.2 V (see Appendix for further information). Therefore, we find the single-electron transfer reaction between O_3 and $HC_2O_4^-$ to be thermodynamically unfavorable, $\Delta G_{26} \sim 96.5$ kJ mol^{-1}. For comparison, the reduction potential for the $^\bullet OH/OH^-$ couple is sufficiently high ($E \sim 1.9$ V[64,65]) for a kinetically viable direct one-electron transfer mechanism. Consequently, the one-electron ozone oxidation of bioxalate, $HC_2O_4^-$, is expected to be a slow reaction, consistent with the upper limit for the bimolecular rate constant reported by Hoigne and Bader, eq 12, 26.[43]

$$K_{12}[O_3 + C_2O_4^{2-}] \leq 4.0 \times 10^{-2}\ M^{-1}\ s^{-1}\ (pH\ 5{-}6) \quad (26)$$

The observed bioxalate degradation rate during ozonolysis is 0.96×10^{-6} M min^{-1}, Figure 2. Using the upper limit from eq 26, $[O_3]_{ss} = 350$ μM, and $[HC_2O_4^-] = 0.9$ mM; an $HC_2O_4^-$ degradation rate of 1.26×10^{-8} M min^{-1} is estimated, which is 76× lesser than the observed rate, indicating a direct electron transfer to O_3 from $HC_2O_4^-$ is too slow to be the primary oxalate decomposition mechanism. In agreement with the zero-order degradation kinetics with respect to oxalate that imply the oxidant as the limiting reagent (i.e., [oxidant] ≪ $[HC_2O_4^-]$, whereas $2.6[O_3] = [HC_2O_4^-]$). Thus, both kinetic and thermodynamic estimations suggest that a direct one-electron oxidation is not the primary oxalate decomoposition pathway during ozonolysis.

In addition to direct reactions with the solute, ozone will decompose in water to yield a number of secondary oxidants such as $^\bullet OH$, $HO_2^\bullet$, $O_2^{\bullet-}$, and $O_3^{\bullet-}$. This decomposition is initiated by the reaction of O_3 with OH^- at a bimolecular rate constant of 70 M^{-1} s^{-1}. Multiple branching pathways yielding various secondary oxidants have been proposed, eq 27.[58,66,67]

$$O_3 + HO^- \rightarrow (O_3^{\bullet -} + HO^{\bullet})/(HOO^{\bullet} + O_2^{\bullet -})/(HO_2^- + O_2) \quad (27)$$

Of these oxy-radical species, only $^{\bullet}OH$ is expected to react with $HC_2O_4^-$ at a non-negligible rate, eq 12. Thus, an upper limit for the bioxalate oxidation rate by secondary ozone oxidants can be estimated assuming $^{\bullet}OH$ is the sole product. If $k_{27} = 70\ M^{-1}\ s^{-1}$, $[O_3]_{ss} = 350\ \mu M$, $[HO^-] = 10^{-11}$ M and $2\ ^{\bullet}OH$ are produced per reaction (the first branching pathway in eq 27), the $^{\bullet}OH$ production rate is estimated to be 5×10^{-13} M s^{-1}. This $^{\bullet}OH$ production rate is 4 orders of magnitude lower than the observed bioxalate ozonolysis degradation rate of 1.6×10^{-8} M s^{-1}, indicating that secondary oxidant production is insufficient to account for the observed decomposition. The absence of a direct or even secondary ozone oxidation mechanism fast enough to comply with observed kinetics, suggests a radical-chain production mechanism. The likely radical-chain mechanism will be discussed in detail in the following section as the third possibility for the synergism of ozone and ultrasound toward bioxalate decomposition.

$HC_2O_4^-$ Oxidation during Sonozone Treatment: Plausible Synergistic Mechanisms. The decomposition rate of $HC_2O_4^-$ during sonozone, combined ultrasound/ozone system, treatment is significantly enhanced (a maximum of 16-fold) compared to the linear addition of the individual rates. The extent of the O_3/US synergism toward oxalate degradation is dependent on both O_3 influx and acoustic power ($^{\bullet}OH$ source), Figure 3. At both ozone concentrations evaluated, increasing the ultrasonic power increases the bioxalate degradation rate to an ozone-dependent plateau, indicating an US-based ozone-decomposition pathway may eventually limit the synergism. More important is a better understanding of the complex O_3−US−bioxalate reaction chemistry that drives the observed synergism, which will allow for optimization of the solution chemistry for the degradation of bioxalate.

The simultaneous application of aqueous ozonolysis and sonolysis has been applied to the degradation and mineralization of a number of organic compounds.[6,33−35,68] In most cases, there is minimal to negligible synergism toward initial organic degradation unless the compound is primarily degraded in the bubble vapor. For example, MTBE degrades in the bubble vapor, and Kang and Hoffmann[79] observed up to 3.9 fold increase in the MTBE degradation rate under similar O_3/US conditions (205 kHz, 200 W/L, [MTBE] = 0.5−1.0 mM, and $[O_3] = 300\ \mu M$). In comparison, studies that focused on compounds that primarily degraded at the bubble-water interface observed enhancements less than a factor of 2 or even negative effects.[6,35,69] By comparison, the 16× increase in bioxalate degradation rates observed upon simultaneous O_3/US is somewhat remarkable, and implies there may be a synergistic mechanism unique to the O_3/US-bioxalate system since bioxalate will be predominantly found in bulk aqueous solution.

The results here are consistent with previous reports on enhanced TOC decomposition rates during sonozone treatment.[33,34,88] The combination of O_3 and US has been observed to have strong synergism toward TOC loss rates. Slow TOC loss rates during ultrasonic irradiation are attributed to the formation of small organic acids such as bioxalate. These small organic acids preferentially partition to the bulk aqueous phase and are relatively stable toward oxidation, yielding them recalcitrant toward ultrasonication or ozonolysis alone. Therefore, when evaluating the following mechanisms, we will assume that the hydroxyl radical ($HO^{\bullet}$) is the only bulk aqueous oxidant produced able to oxidize bioxalate. For example, during ultrasound alone, the steady-state concentration of $HO^{\bullet}$ has been estimated to be 5.4×10^{-13} M, and a similar steady-state $HO^{\bullet}$ would be required during ozonolysis. Thus, the observed rate increase during simultaneous ozonolysis and ultrasonic irradiation would require a steady-state $HO^{\bullet}$ concentrations of 8×10^{-12} M, over an order of magnitude greater.

In the following sections, 3 plausible mechanisms for the enhanced hydroxyl radical production during O_3/US treatment will be evaluated: (I) sonochemical decomposition of O_3 within collapsing bubbles to produce $HO^{\bullet}$, (II) reactions of O_3 with sonochemically produced H_2O_2 to produce $HO^{\bullet}$, and (III) a radical chain mechanism via O_2-mediated $CO_2^{\bullet -}$ reduction of O_3 to produce $HO^{\bullet}$. Estimations of the maximal possible increase in bulk $HO^{\bullet}$ will be utilized to evaluate if the mechanism is viable for the observed synergism.

Mechanism I: $^{\bullet}OH$ Production via Sonochemical Decomposition of O_3. The pyrolytic decomposition of gaseous ozone within transiently cavitating bubbles may indirectly produce increased concentrations of the hydroxyl radical. The thermal decomposition of O_3 yields molecular O_2 and triplet atomic oxygen, eq 28. And the subsequent high-temperature reaction of the $O(^3P)$ with water, eq 29, yields $2HO^{\bullet}$.

$$O_3 \xrightarrow{)))\Delta} O_2 + O(^3P) \quad (28)$$

$$O(^3P) + H_2O \rightarrow 2\ ^{\bullet}OH \quad (29)$$

The sequence of eqs 28 and 29 could possibly yield greater hydroxyl radical concentrations; however, a 16× increase may be unattainable. Acoustic caviation simulations report that the gaseous bubble has been estimated to fractionally contain 10−30% water vapor, and a large fraction of this water vapor is homolyzed, eq 10, during collapse. Thus, the addition of 3% ozone (i.e., O-atom during collapse) may yield only minor increases to bulk hydroxyl radical yield. $O(^3P)$ will also react with a number of the other radical species produced in the bubble vapor, such as O, $HO^{\bullet}$, $HO_2^{\bullet}$, H_2O_2, O_2, and will also destroy O_3, eq 30.

$$O_3 + O(^3P) \xrightarrow{)))\Delta} 2O_2 \quad (30)$$

Thus, the absolute increase in bulk $HO^{\bullet}$ due to O_3 decomposition in the cavitating bubble vapor may not be sufficient for the observed synergism during bioxalate degradation.

The results of previous studies on US and US/O_3 hydrogen peroxide yields support this statement. The sonolysis of aqueous ozone (3% in O_2) enhances the yield of H_2O_2 compared to O_2-saturated water.[35,69] In the absence of scavengers, the predominant stable product of the sonolysis of water is H_2O_2 which results from the self-termination reactions of the hydroxyl, eq 31, and the hydroperoxy/superoxide radicals, eqs 19 and 20.

$$^{\bullet}OH + {}^{\bullet}OH \rightarrow H_2O_2 \quad (31)$$

Using the production rates of H_2O_2 as an indirect measure of free radical production, these studies suggested that the enhanced OH production results from the thermal decomposition of ozone inside the cavitation bubbles. However, the maximum O_3/US

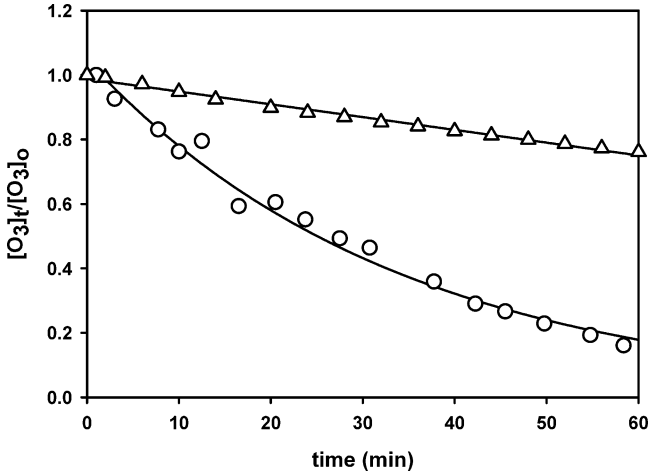

Figure 4. Ozone decay in ultrapure water ($[O_3]_0 = 100\ \mu M$, 0.605 L, 15 °C, $pH_{initial} \sim 5$). Δ: in pure water; ○: ultrasound is applied at $t = 0$ (358 kHz, 10 W).

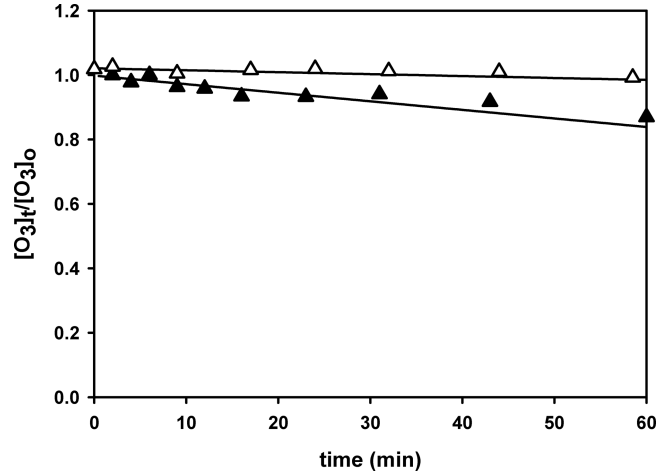

Figure 5. Ozone decay in ultrapure water. ($[O_3]_0 = 100\ \mu M$, 0.605 L, 15 °C, $pH_{initial} \sim 3$). Δ: in pure water; ▲: oxalic acid is added at $t = 0$ ($[H_2C_2O_4]_o = 0.9$ mM).

H_2O_2 production enhancement observed was only 3× greater than US alone, and in all cases the O_3 decomposition rate was greater than the H_2O_2 production rate, indicating that only a fraction of the ozone decomposed in the bubble vapor may yield hydroxyl radicals. These results are consistent with reports on the degradation of PCP,[6] 4-nitrophenol, nitrobenzene, 4-chlorophenol,[69] and phenol[88] by the sonozone process. Only small (<2×) enhancements over US or O_3 decomposition rates were observed for these species that should primarily degrade oxidatively at the bubble-water interface.

To experimentally verify whether this mechanism could account for the enhanced degradation of $HC_2O_4^-$ in the combined system, batch ozone decay experiments were conducted in the presence and absence of both oxalic acid and ultrasonic irradiation. As shown in Figure 4, the silent (i.e., nonacoustic) decay of ozone ($[O_3]_0 \sim 100\ \mu M$) in pure water at pH 5 results in a ~ 25% loss within the first hour. This decay followed zero-order kinetics with a rate of $d[O_3]/dt = 0.4\ \mu M\ min^{-1}$, indicating a radical chain decomposition mechanism since the reaction of O_3 with HO^-, eq 27, is kinetically insufficient to account for the decomposition. Application of ultrasound (358 kHz, 10 W, 16.7 WL^{-1}) to the same ozone solution increased the initial rate of O_3 decay to $\sim 1.6\ \mu M\ min^{-1}$, open circles in Figure 4. Ultrasonic irradiation resulted in an exponential decrease of ozone with sonication time with an apparent first-order rate constant of $k_{1,-O_3} = 0.032\ min^{-1}$ over more than three half-lives. Previous studies have also observed enhanced apparent first-order ozone decay kinetics in the presence of ultrasonic irradiation and attributed the decomposition to sonolytic degradation and degassing.[35,44,70] The direct pyrolysis of gaseous ozone is expected to lead to zero-order degradation kinetics since ozone is present in relatively low concentrations in the feed gas ($O_3/O_2 < 0.05$) and cavitation dynamics are not expected to change significantly with changes in ozone concentration.[71] However, ozone will also react with a number of species such as $^{\bullet}OH$, eq 32, or HO_2^-.

$$O_3 + {}^{\bullet}OH \rightarrow HO_2^{\bullet} + O_2 \qquad (32)$$

The reported bimolecular rate constant for this reaction is $k_{32} = 1.1 \times 10^8\ M^{-1}\ s^{-1}$,[72] which suggests that reaction 32 could lead to increased ozone degradation in the bubble vapor, interface and in bulk solutions. As ozone concentrations are reduced, this process would compete with other reactions such as the self-reaction of the hydroxyl radical (eq 31, $k_{37} = 5.5 \times 10^9\ M^{-1}\ s^{-1}$), resulting in the apparent first-order degradation kinetics for ozone.

The addition of oxalic acid to an aqueous solution depressed the pH from ~ 5 to 3. No decay was observed for solutions of ozone dissolved in pure water adjusted to pH 3 with perchloric acid, Figure 5. Thus, even though HO^- may not be responsible for the direct decomposition of O_3 in solution, eq 27, the reaction is the likely initiator of the radical-chain responsible for the observed decomposition. This observation is in agreement with current ozone kinetic models, which propose that the decay of aqueous ozone is initiated by OH^- attack and proceeds via a free radical pathway.[58,66] As shown in Figure 5, addition of oxalic acid accelerates the degradation of ozone, and 87% of the initial ozone remained in solution after 1 h of reaction. This finding is consistent with previous findings[73] that reported slow oxidation of oxalic acid by O_3 at pH 3.5. Ozone decay follows apparent zero-order kinetics with a decay rate of $0.22\ \mu M\ min^{-1}$, which is similar to the bioxalate decay of $0.25\ \mu M\ min^{-1}$ under the same reaction conditions. The similar ozone-to-bioxalate decay rates would seemingly imply a direct oxidation reaction, but our kinetic estimations using eq 26 were much too slow for this to be feasible. This suggests that O_3 may react with an bioxalate degradation intermediate.

As noted above, oxalate does not react at a significant rate with ozone, and the presence of oxalate is not expected to enhance the cavitational efficiency of the acoustic field. Thus, if the enhanced production of $^{\bullet}OH$ in the O_3/US system resulted only from the pyrolytic decomposition of ozone, then ozone decomposition in the experiments should be unaffected by the addition of oxalic acid. In addition, if ozone decomposition primarily results from $^{\bullet}OH$ attack in bulk solution, then oxalic acid would compete for this radical species, eq 12, and be expected to decrease ozone decay rates. However, the addition of oxalic acid to an ultrasonically irradiated ozone solution increased the O_3 decay rate to $3.5\ \mu M\ min^{-1}$, more than doubling the initial loss rate compared to sonication alone, Figure 6. The increase in ozone decomposition kinetics upon oxalate addition is more impressive considering the sonication alone was completed at pH 5 and the combined experiment at pH 3. In addition, the presence of oxalic acid also shifted the kinetic order of the reaction from apparent first-order to zero-order.

The addition of oxalate increased ozone decomposition rates both in the presence and absence of sonication, indicating that

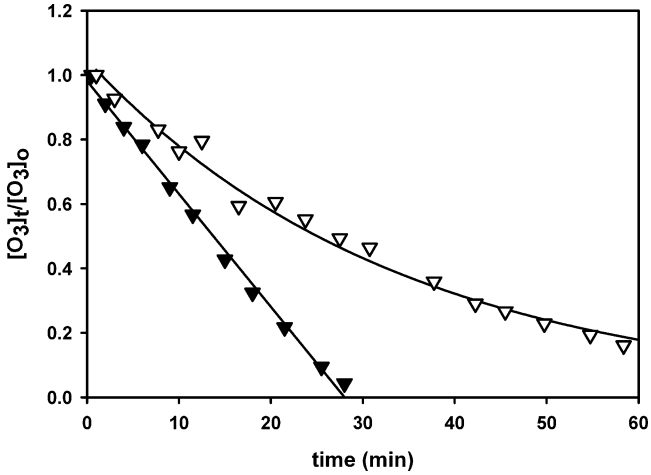

Figure 6. Ozone decay in ultrapure water in the presence of ultrasound irradiation applied at $t = 0$. ($[O_3]_0 = 100\ \mu$M, 358 kHz, 10 W, 15 °C) ▽: in neat water ($pH_{initial} \sim 5$), ○ in Figure 4; ▼: $[H_2C_2O_4]_0 = 0.9$ mM added at $t = 0$ ($pH_{initial} \sim 3$).

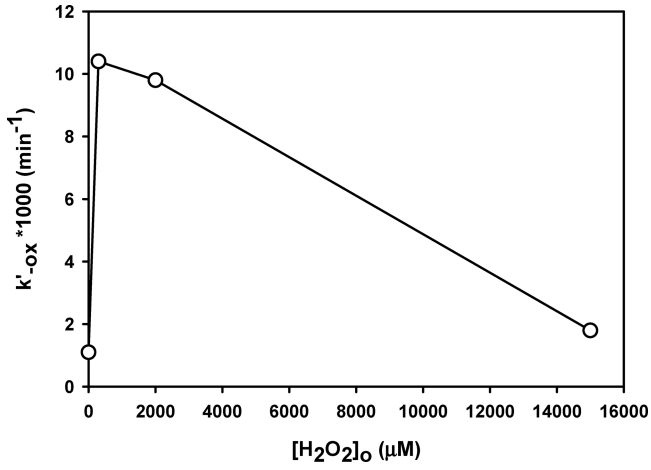

Figure 7. Normalized pseudozero-order degradation rate constants of $[H_2C_2O_4]_t$ with ozone and H_2O_2 ($[O_3]_{ss} = 350\ \mu$M, $[C_2H_4O_4]_0 = 0.9$ mM, 0.605 L, 15 °C, pH ~ 3).

oxalate or an oxalate oxidation intermediate is primarily responsible for the observed ozone degradation. This is inconsistent with mechanism I that O_3 decomposition in acoustically cavitating bubbles can yield increased bulk hydroxyl radical concentrations responsible for the observed bioxalate degradation rates in the O_3/US system. This is in agreement with previous reports on enhanced H_2O_2 production during simultaneous ozonolysis and sonication being insufficient to explain the results observed here. Therefore, we conclude mechanism I may be responsible for slight enhancements in bulk hydroxyl radical concentrations, but can not explain the synergistic 16× increase in bioxalate degradation rates.

Mechanism II: •OH Production via O_3/H_2O_2 Reactions. Kang and Hoffmann[74] also found mechanism I to be insufficient to account for their observations during the combined ozonolysis and ultrasonic irradiation of methyl *tert*-butyl ether. They proposed that in addition to the direct pyrolysis of ozone, the enhanced oxalate kinetics in the O_3/US system may arise from ozone reactions with H_2O_2. Previous reports have shown that adding H_2O_2 to aqueous O_3 solutions significantly increased oxidation kinetics of a number of organic substrates,[67,75−77,70] including oxalic acid.,[73,78] and the sonolysis of water is known to produce significant concentrations of hydrogen peroxide.[42,51,70,79] Experiments performed in identical ultrasonic reactors operating at similar power densities and frequencies to our system have estimated the sonochemical production rate of hydrogen peroxide to be 1.5−3 μM min^{-1}.[42,70] H_2O_2 does not react directly with O_3. The deprotonated form, HO_2^-, does react with aqueous ozone via a similar mechanism to HO^-, but at a significantly faster rate ($k_{34} = 2.8 \times 10^6$ M^{-1} s^{-1}).[58,66] Staehelin and Hoigne[58] have proposed that the reaction between HO_2^- and O_3, eq 34, initiates a free radical chain which ultimately produces •OH.

$$HO_2^- + H^+ \rightarrow H_2O_2\ (pK_a = 11.8) \quad (33)$$

$$O_3 + HO_2^- \rightarrow HO_3^\bullet + O_2^{\bullet -} \quad (34)$$

$$O_3 + HO_2^\bullet/O_2^\bullet \rightarrow HO_3^\bullet/O_3^{\bullet -} + O_2 \quad (35)$$

$$HO_3^\bullet \leftrightarrow O_3^{\bullet -} + H^+ \quad (36ab)$$

$$HO_3^\bullet \rightarrow {}^\bullet OH + O_2 \quad (37)$$

Kinetic isotope effects[80] indicate that the reaction between O_3 and HO_2^- does not produce free radicals but proceeds via a hydride transfer into a closed-shell trioxide species, HO_3^-

$$O_3 + HO_2^- \rightarrow HO_3^- + O_2 \quad (38)$$

The reactivity of this intermediate species is not very well understood. Initial reports have suggested that HO_3^-/H_2O_3 may act as a mild oxidizing reagent.[81,82] The contribution of this mechanism will be limited by the low pH of the reaction solution. For example, if $[H_2O_2]_{tot} = 10^{-5}$ M, then at pH 3: $[HO_2^-] = 10^{-13.8}$ M and $\tau_{1/2}(O_3 + HO_2^-) = 1.6 \times 10^7$ s, and pH 5: $[HO_2^-] = 10^{-11.8}$ and $\tau_{1/2}(O_3 + HO_2^-) = 1.6 \times 10^5$ s, both estimated half-lives are greater than the total reaction time.

To evaluate whether H_2O_2 may enhance bioxalate ozonolysis rates, decomposition experiments were completed in the absence of ultrasonication, Figure 7. The addition of 300 and 2000 μM H_2O_2 to an ozone-saturated solutions ($[O_3]_{ss} = 350\ \mu$M) increased degradation rates nearly 10-fold compared to ozonolysis alone, with a pseudofirst-order rate constant of ${}^{H_2O_2-O_3}k'_{-ox} = 1.0 \times 10^{-5}$ min^{-1}. The kinetic enhancement over ozonolysis alone is likely due to the initiation of the radical-chain depicted in eqs 33−38. Thus, the reaction of O_3 with H_2O_2 is able to increase bioxalate degradation kinetics to a similar extent as the combined O_3/US system. However, it would require tens of hours of ultrasonication to yield the hydrogen peroxide levels necessary to achieve the observed rate increases in Figure 7, even with simultaneous ozonolysis. Since these experiments were not completed with simultaneous ultrasonication, this does not rule out a process occurring during ultrasonication that can not be accounted for with just adding H_2O_2.

To assess if the enhanced reactivity was resulting from a sonochemically based process, ozone solutions were prepared with simultaneous low-power ultrasonic irradiation for 1 h prior to removal of the ozone source. Two cases are presented in Figure 8, one where the ultrasonic irradiation is continued after the ozone source was removed and one where the ultrasonic irradiation is discontinued. In both presonication cases, ozone decomposition was faster as compared to solutions prepared under acoustically "silent" conditions, Figure 6. The presonication increased the initial ozone decay rate, 6.4 μM min^{-1}, to

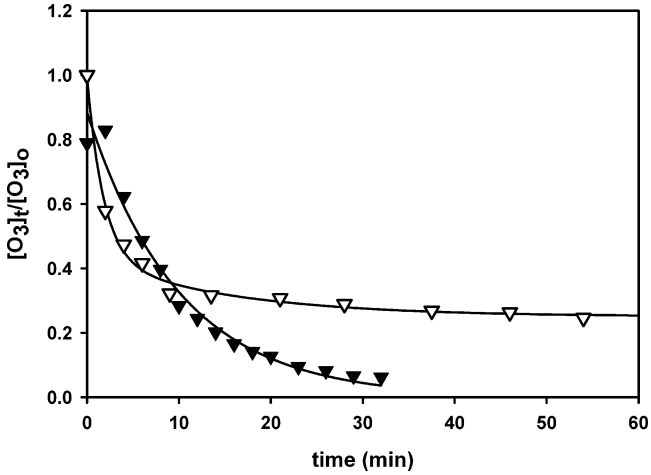

Figure 8. Ozone decay in ultrapure water. Ozone solution is presonicated for 1 h prior to $t = 0$ ($[O_3]_0 = 100\ \mu M$, 358 kHz, 10 W, 0.605 L, 15 °C, $pH_{initial} \sim 5$). ▼: acoustic source remains on after $t = 0$; ▽: acoustic field is removed at $t = 0$.

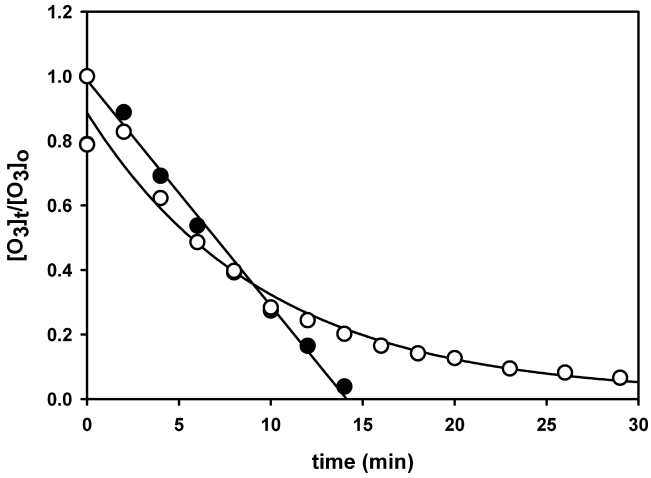

Figure 9. Ozone decay in ultrapure water. Ozone solution is presonicated for 1 h prior to $t = 0$. The acoustic field remains on after $t = 0$. ($[O_3]_0 = 100\ \mu M$, 358 kHz, 10 W, 0.605 L, 15 °C). ○: in neat water ($pH_{initial} \sim 5$), ▼in Figure 7; ●: $[H_2C_2O_4]_o = 0.9$ mM added at $t = 0$ ($pH_{initial} \sim 3$).

nearly 4 times that of solutions irradiated only after the removal of the ozone source. In both cases, the accelerated ozone decomposition rate was active for the first 10 min of reaction, and thereafter the decay rate decreased substantially and to a greater extent in the case of discontinued sonication where it was reduced to $-d[O_3]/dt \sim 0.14\ \mu M\ min^{-1}$.

These findings indicate that relatively long-lived intermediate products capable of reacting with ozone are formed during the ultrasonic irradiation of ozone saturated solutions. It is most likely that HO_2^-, which results from the dissociation of sonically generated H_2O_2 is reacting with the ozone via reactions 34 and 38. We previously reported[80] that the stoichiometry of the peroxone reaction to vary between $\Delta O_3/\Delta H_2O_2 = 2.7$ and 7.1. Figure 8 indicates a loss of $\sim 70\ \mu M\ O_3$, which corresponds to $[H_2O_2]_0$ between 10 and 25 μM. These H_2O_2 concentrations are consistent with the sonochemical production of H_2O_2 reported by Kang and Hoffmann.[74]

As shown in Figures 9 and 10, the addition of oxalic acid after presonication of ozone solutions enhanced the ozone decay mechanism when irradiation continued during the experiment. While initial decay rates were not altered significantly, enhanced degradation was observed after 10 min of insonation, suggesting

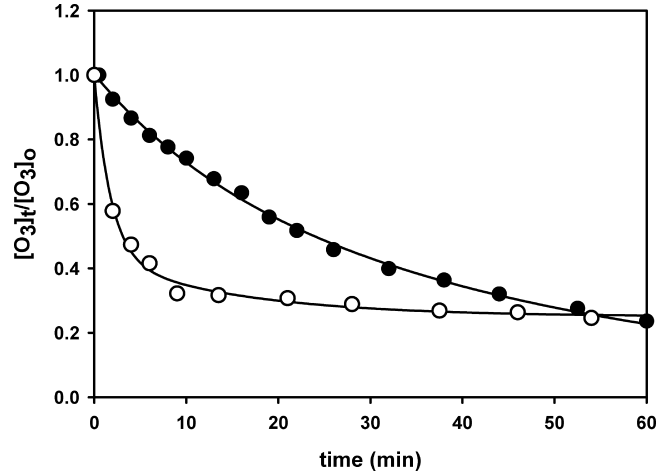

Figure 10. Ozone decay in ultrapure water. Ozone solution is presonicated for 1 h prior to $t = 0$. The acoustic field is turned off after $t = 0$. ($[O_3]_0 = 100\ \mu M$, 358 kHz, 10 W, 0.605 L, 15 °C). ○: in neat water ($pH_{initial} \sim 5$); ●: $[H_2C_2O_4]_o = 0.9$ mM added at $t = 0$ ($pH_{initial} \sim 3$).

that oxalate or an oxalate oxidation intermediate is involved in a radical-chain production mechanism. However, when sonolysis was halted concurrently with the start of the kinetic run, Figure 10, the presence of oxalate actually inhibited the degradation of ozone compared to experiments performed in neat water. This observation is most likely not the result of a competitive reaction between $HC_2O_4^-$ for reactive species generated by the sonozone treatment, but rather can be attributed to the pH drop within the solution from pH 5 to ~3 upon addition of $H_2C_2O_4$. The decrease in pH effectively lowers the $[HO_2^-]_{ss}$ by 2 orders of magnitude, significantly slowing the degradation of ozone by eqs 34, 38, and the radical-chain found in eqs 33 and 35−37.

It is obvious that presonication increases the initial ozone decomposition rate due to production of HO_2^-, but does the increased ozone decomposition rate have any effect on the oxalic acid decomposition rate (i.e., does the increased ozone decomposition rate lead to a significant increase in the steady-state hydroxyl radical concentration?)? To determine whether additional H_2O_2/O_3 reactions could account for the strong synergism of the combined system for the oxidation of $HC_2O_4^-$, separate oxalate degradation experiments were performed using presonicated ozone solutions. Ozone saturated water $[O_3]_{ss} = 150\ \mu M$ was irradiated at 358 kHz at several acoustic powers ranging from 0−100 W for an hour prior to the addition of oxalate. Degradation rates in the presonicated solutions were nearly identical to the rates obtained when ultrasonic irradiation commenced at $t = 0$, Figure 11. A similar lack of enhancement is shown in Figure 12, when H_2O_2 was spiked along with oxalic acid to a combined ozone/ultrasound system. (358 kHz, 100 W, $[O_3]_{ss} = 150\ \mu M$, $[H_2O_2]_o = 50$, 112, and 300 μM. $[H_2C_2O_4]_o = 0.9$ mM) Figure 12 also indicates that at excessive (~2 mM) concentrations of H_2O_2, the degradation of $HC_2O_4^-$ can actually be inhibited. This is the result of $^{\bullet}OH$ scavenging by H_2O_2 to produce the essentially unreactive hydroperoxyl radical, $HO_2^{\bullet}$, eq 39.

$$H_2O_2 + {}^{\bullet}OH \rightarrow HO_2^{\bullet} + O_2 \qquad (39)$$

The bimolecular rate constant of this reaction is reported[83] as $k_{40} = 2.7 \times 10^7\ M^{-1}\ s^{-1}$. The scavenging of $^{\bullet}OH$ by H_2O_2 should become competitive with its reaction with $HC_2O_4^-$, eq

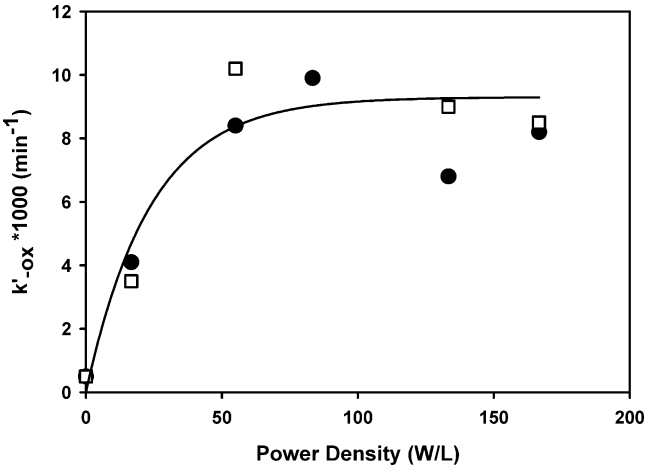

Figure 11. Normalized pseudozero-order degradation rate constants of $[H_2C_2O_4]_t$ with ozone and ultrasound as a function of ultrasonic acoustic power. □: ultrasound pre-equilibrated with ozone 1 h prior to the addition of oxalic acid; ●: ultrasound added simultaneously with the addition of oxalic acid. ($[O_3]_{ss}$ =150 μM, 358 kHz, $[C_2H_4O_4]_0$ = 0.9 mM, 0.605 L, 15 °C, pH ~ 3).

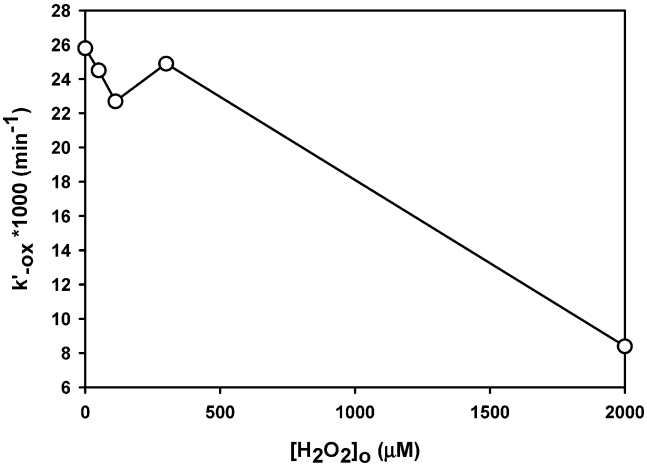

Figure 12. Normalized pseudozero-order degradation rate constants of $[H_2C_2O_4]_t$ with ozone, ultrasound, and H_2O_2. ($[O_3]_{ss}$ =300 μM, 358 kHz, 100 W, $[C_2H_4O_4]_o$ = 0.9 mM, 0.605 L, 15 °C, pH ~ 3).

12, ($k_{12} = 4.7 \times 10^7$ M^{-1} s^{-1}) when $[H_2O_2]_0 \geq 1.5$ mM, which is in agreement with our experimental findings. Thus, from the experimental results of Figures 7−12 we conclude that the reaction of O_3 and H_2O_2 will increase ozone decomposition rates, but the ozone decomposition via this mechanism will not increase bulk hydroxyl radical concentrations to the extent required to observe increases in the bioxalate degradation rate.

Mechanism III: Radical Chain •OH Production from CO_2. With mechanisms I and II already seemingly ruled out, this leaves mechanism III to explain the synergism observed in the O_3/US degradation of oxalic acid. In all the systems, US/O_3/US+O_3, $HC_2O_4^-$ will be oxidized to $CO_2^{\bullet-}$ via reaction with HO•, eqs 12 and 26. In the US system, $CO_2^{\bullet-}$ will react with O_2 to yield $O_2^{\bullet-}$, eq 17, which proceeds through chain termination reactions, eqs 18−20, to produce H_2O_2. However, in the presence of O_3, $O_2^{\bullet-}$ will predominantly react at diffusion-controlled rates with the relatively high concentration ozone, eq 35, and subsequently produce •OH via eq 37b then 38. This leads to an •OH radical-chain mechanism, Scheme 1, leading to enhanced $HC_2O_4^-$ degradation kinetics. This radical chain is expected to be present in both O_3 and US/O_3 systems.

SCHEME 1: Depiction of Radical-Chain Propagation (Green) and Termination (Red) Reactions That Mediate the O_3/US Synergism Towards Bioxalate Degradation

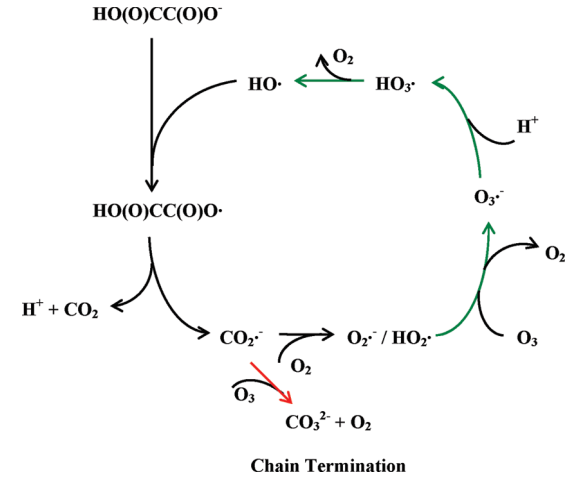

In addition to reaction of $CO_2^{\bullet-}$ with O_2, the carboxyl anion radical may also undergo a one-electron transfer with ozone to produce the ozonide radical, eq 40.

$$CO_2^{\bullet-} + O_3 \rightarrow CO_2 + O_3^{\bullet-} \qquad (40a)$$

Reaction 40a followed by reactions 37b and 38 will also regenerate •OH in a similar radical chain propagating reaction. Alternatively, the reaction of $CO_2^{\bullet-}$ and O_3 may occur through an O-atom transfer to yield bicarbonate, eq 40b, a chain-termination reaction.

$$CO_2^{\bullet-} + O_3 \rightarrow CO_3^{2-} + O_2 \qquad (40b)$$

If the chain-propagating reaction 40a was the dominant $CO_2^{\bullet-}$ and O_3 branching pathway, then HOO•/$O_2^{\bullet-}$ recombination, eqs 18−20, would be the major chain-terminating reaction.

To evaluate if the radical chain depicted in Scheme 1 is plausible for the observed synergism, we will estimate its chain length. Assuming O_2 is the primary scavenger of $CO_2^{\bullet-}$, the •OH radical chain length can be estimated by calculating the ratio of propagation rates, eq 35, to termination rates, eq 19−20 or $l_{chain} = k_{35}\,[O_3]_{ss}/2(k_{19/20})[HO_2]_{ss}$. Estimations of pH dependence of the rate constants[50,84] can be made as follows: ${}^{pH}k_{35} = k_{35}\,(10^{-pK_a}/(10^{-pH} + 10^{-pK_a})$ and ${}^{pH}k_{19/20} = (k_{19} + k_{22}\,(K_{HO_2}/[H^+]))/(1 + K_{HO_2}/[H^+])^2$ while $[HO_2]_{ss}$ can be estimated from the OH production rates $P_{OH} = 2^{pH3}k_{19/20}\,[HO_2]^2_{ss}$ yields ${}^{pH3}k_{35} = 2.5 \times 10^7$ M^{-1} s^{-1}, ${}^{pH3}k_{19/20} = 2.45 \times 10^6$, and $[HO_2]_{ss} = 5 \times 10^{-8}$ M, respectively. The radical-chain length, L_{chain}, is then calculated to be 3.5×10^4. The determined radical chain length is orders of magnitude more than sufficient to explain the observed synergism and is definitely the most viable candidate of the three mechanisms proposed. Actually, the estimated chain length is unattainably high and suggests that the reaction $CO_2^{\bullet-}$ + O_3 may be a chain termination that controls the otherwise explosive chain.

Examination of the Proposed O_3/US Mechanism of Synergism. ***Facsimile Kinetic Simulations.*** To further examine whether mechanism III can explain the O_3/US synergism, kinetic simulations were made using FACSIMILE. The overall chemical mechanism was assembled from a mechanism utilized in our[80] previous simulations with the addition of reactions of the carbon

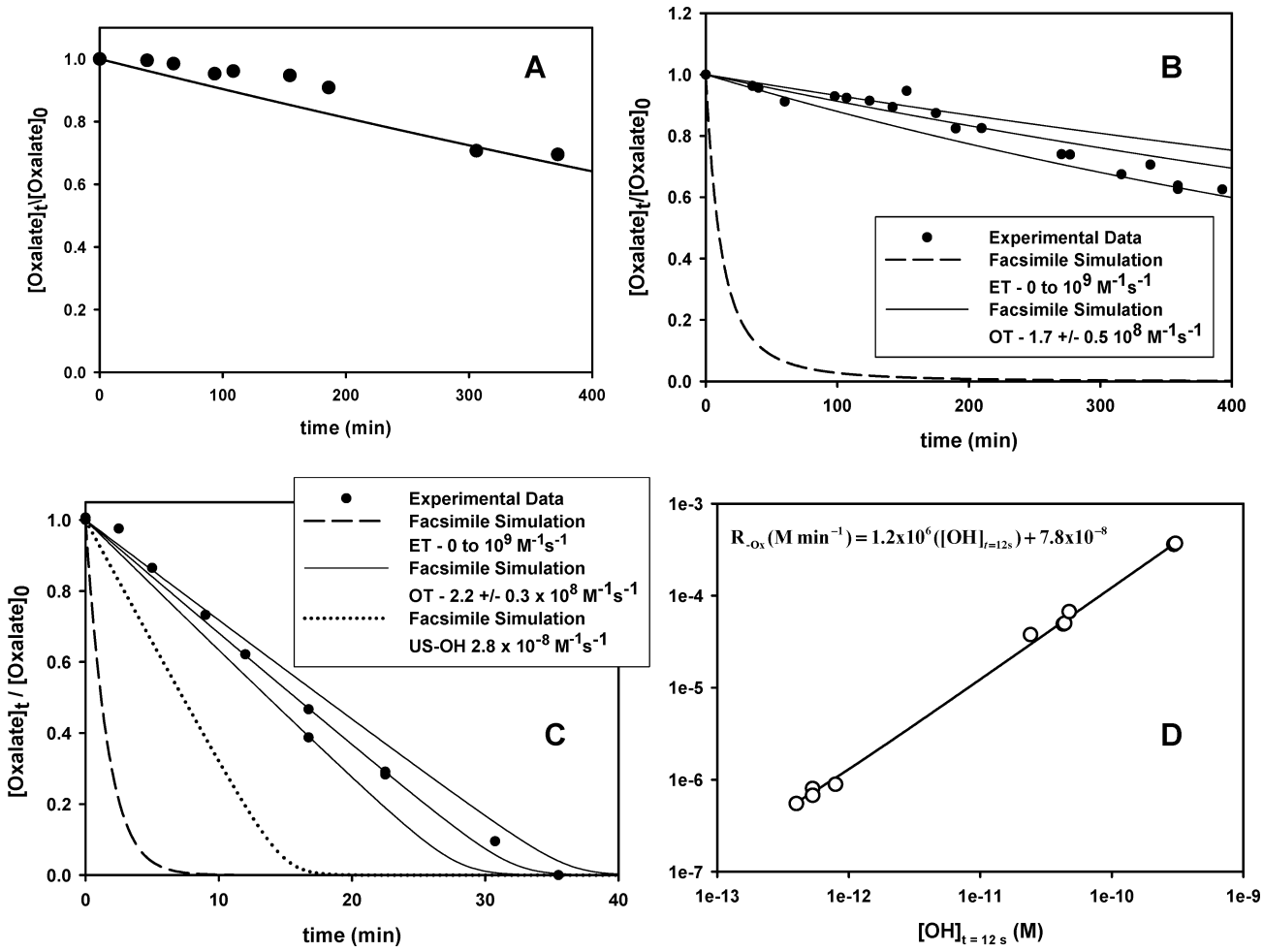

Figure 13. Kinetic simulations of experimental kinetics; (●) experimental data and lines are simulations utilizing different kinetic mechanisms and rate constants. (a) US only, (b) O_3 only, (c) US/O_3, and (d) simulated oxalate degradation rates vs [OH] at $t = 12$ s.

dioxide radical, Table 1. $CO_2^{\bullet-}$ is assumed to be the only form of the carbon dioxide radical. Initial concentrations were $[HC_2O_4^-]_0 = 0.9$ mM, $[H^+] = 1$ mM, and $[OH^-] = 10^{-11}$ M. Ozone and oxygen were treated as constants since they were continuously sparged into the aqueous solution. The rate of ozone reacting with $HC_2O_4^-$ is taken to be the upper limit determined from our estimations, 5×10^{-4} M^{-1} s^{-1}. The specific products of the reaction of O_3 and OH^- had no effect on the oxalate degradation kinetics. The reaction mechanism and rate of O_3 with $CO_2^{\bullet-}$ was evaluated by the simulations and will be discussed further.

The initial kinetic simulations were completed on the degradation of bioxalate by ultrasound. $^{\bullet}OH$ production by ultrasound was set to 1.4×10^{-8} M^{-1} s^{-1}. The results are plotted in Figure 13a. The experimental results are well fit by the kinetic simulations.

The next kinetic simulations were an attempt at fitting the degradation of bioxalate by ozonolysis, Figure 13b. A number of kinetic simulations were completed as an attempt to determine the mechanism and kinetics of the reaction of O_3 and $CO_2^{\bullet-}$. Numerical simulations were completed using a wide range of rate constants from 0 to 10^9 M^{-1} s^{-1} for the electron transfer mechanism, eq 40a, keeping the rate constant for the O-atom transfer pathway, eq 40b, equal to 0. In all cases, the simulated oxalate degradation curves were identical and much faster than the experimentally observed kinetics, dashed line in Figure 13b. This is consistent with the estimation of the radical chain length assuming the reaction of O_3 and $CO_2^{\bullet-}$ a chain propagating electron transfer. Kinetic simulations were then completed with a range of rate constants assuming the reaction of O_3 and $CO_2^{\bullet-}$ was a chain terminating O-atom transfer. The solid lines represent simulations made using $k_{36a} = 0$ and $k_{36b} = 1.7 \pm 0.5 \times 10^8$ M^{-1} s^{-1}, Figure 13b.

The kinetic simulations of bioxalate degradation using simultaneous ultrasound and ozonolysis are shown in Figure 13c. The solid lines are simulations with the reaction of O_3 and $CO_2^{\bullet-}$ as an O-atom transfer with a second-order rate constant of $k_{36b} = 2.2 \pm 0.3 \times 10^8$ M^{-1} s^{-1} and OH production by ultrasound set to 1.4×10^{-8} M^{-1} s^{-1}. The second-order rate constant for the reaction of O_3 and $CO_2^{\bullet-}$ is similar to the rate constant obtained from the simulation of ozonolysis alone. As a test of mechanism I, the ultrasonic bulk aqueous $^{\bullet}OH$ production rate was doubled to 2.8×10^{-8} M^{-1} s^{-1} as indicated with the dotted line of Figure 13c. However, the simulated kinetics at this higher $^{\bullet}OH$ production rate do not conform to the observed reaction kinetics.

The initial bioxalate degradation rate, R_{-Ox}, for the all the simulations is plotted in log−log format against $^{\bullet}OH$ concentrations at the first simulation time point, $t = 12$ s, Figure 13d. There is a linear correlation between the degradation rate and [$^{\bullet}OH$], indicating that the hydroxyl radical is the primary bioxalate oxidant in all cases. The results from the kinetic simulations support the mechanism depicted in Scheme 1. After initial oxidation of bioxalate, $HC_2O_4^-$, the resulting carbon dioxide radical, $CO_2^{\bullet-}$, has a chain-propagating and chain-terminating branching pathway. The chain propagating pathway,

green, involves a reaction with oxygen, O_2, to yield superoxide, $O_2^{\bullet-}$, which in turn reacts with ozone, O_3, to yield ozonide, $O_3^{\bullet-}$, which upon protonation unimolecularly decomposes to yield a hydroxyl radical, $^{\bullet}OH$. The chain termination pathway, red, involves reaction of $CO_2^{\bullet-}$ with O_3 which yields carbonate, CO_3^{2-} and oxygen, O_2. The ratio of aqueous O_2 to O_3 will determine the chain length of the reaction and in the current system is around 4.

Conclusions

This study demonstrates that the combination of ozonolysis and ultrasound is able to degrade aqueous oxalate more efficiently than predicted by the simple linear addition of two independently reacting systems. Ozone decay experiments suggest that the apparent rate enhancements are the result of a reaction between the carbon dioxide radical anion and molecular ozone. This reaction effectively increases the yield of hydroxyl radical which is known to rapidly oxidize oxalate.

Appendix

Thermochemical Considerations

The oxidation half-reaction of bioxalate to its corresponding radical is given by

$$HC_2O_4^- \rightarrow HO(O)C{-}C(O)O + e^- \quad \text{(A1)}$$

The oxidation potential for reaction 1, E_1 can be expressed as

$$E_1 = \frac{-\Delta_r G_1}{nF} \quad \text{(A2)}$$

where n is the number of electrons, F is the Faraday constant, and $\Delta_r G_1$ is the standard Gibbs energy for reaction 1. $\Delta_r G_1$ is given by the difference in standard Gibbs energies, $\Delta_f G$, of the products and the reactants

$$\Delta_r G_1 = \Delta_f G(HO(O)C{-}C(O)O^{\bullet}) - \Delta_f G(HC_2O_4^-) \quad \text{(A3)}$$

We can estimate the value of $\Delta_r G_1$ as follows:

The H-bond dissociation of oxalic acid will produce the bioxalate radical

$$H_2C_2O_4 \rightarrow HO(O)C{-}C(O)O^{\bullet} + H^{\bullet} \quad \text{(A4)}$$

The acid-dissociation of oxalic acid will yield bioxalate

$$H_2C_2O_4 \rightarrow HO(O)C{-}C(O)O^- + H^+ \quad \text{(A5)}$$

An electron transfer from bioxalate to a proton will also produce the bioxalate radical

$$HO(O)C{-}C(O)O^- + H^+ \rightarrow HO(O)C{-}C(O)O^{\bullet} + H^{\bullet} \quad \text{(A6)}$$

From the above reactions the following relationship is obtained:

$$\Delta_r G_1 = \Delta_r G_6 - \Delta_f G(H^{\bullet}) + \Delta_f G(H^+) = \Delta_r G_4 - \Delta_r G_5 - \Delta_f G(H^{\bullet}) + \Delta_f G(H^+) \quad \text{(A7)}$$

where $\Delta_f G(H^+) = 0$ kJ mol^{-1},[85] $\Delta_f G(H^{\bullet}) = 203.25$ kJ mol^{-1},[85] $\Delta_r G_4 \sim 405$ kJ mol^{-1}, and $\Delta_r G_5 \sim 7.0$ kJ mol^{-1} (see calculations for $\Delta_r G_4$ and $\Delta_r G_5$ at the end of this discussion). From eq 7, we estimate $\Delta_r G_1 = 195$ kJ mol^{-1}. Given eq 2 with $F = 96\,485$ C mol^{-1}, $n = 1$, and $\Delta_r G_1 = 195$ kJ mol^{-1}, we calculate that $E_1 = 2.0$ V.

Calculating $\Delta_r G_4$

The standard Gibbs energy for reaction A4, $\Delta_r G_4$, can be expressed as

$$\Delta_r G_4 = \Delta_r H_4 - T\Delta_r S_4 \quad \text{(A8)}$$

where $\Delta_r H_4$ is the enthalpy for reaction 4, $\Delta_r S_4$ is the entropy of reaction 4, and T is the temperature. $\Delta_r H_4$ can be approximated by considering the H-bond dissociation energy of acetic acid, $\Delta_r H_4 \sim \Delta H_{BDE}$ (CH_3CO_2H) = 442.2 kJ mol^{-1}.[86] The change in entropy in reaction 1 should not vary significantly from the entropy changes observed in the H-bond dissociation of formic acid as follows:

$$\Delta_r S_4 \sim \Delta_r S_{BDE}(HCOOH) = \Delta S(HCOO^{\bullet}) + \Delta S(H^{\bullet}) - \Delta S(HCOOH) \quad \text{(A9)}$$

where $\Delta S(HCOO^{\bullet}) = 248.3$ J K^{-1} mol^{-1},[87] $\Delta S\,(H^{\bullet}) = 114.7$ J K^{-1} mol^{-1},[85] and ΔS (HCOOH) = 239.5 J K^{-1} mol^{-1}.[87] Thus, $\Delta_r S_4 = 123.5$ J K^{-1} mol^{-1}. Furthermore, with $\Delta_r H_4 = 442.2$ kJ mol^{-1}, $\Delta_r S_4 = 123.5$ J K^{-1} mol^{-1} and $T = 298$ K, we estimate $\Delta_r G_4 = 405$ kJ mol^{-1}.

Calculating $\Delta_r G_5$

The Gibb's free energy of reaction 5 is related to the acid equilibrium constant, K_a, by

$$\Delta_r G_5 = -RT \ln K_a \quad \text{(A10)}$$

With the p$K_a = 1.23$, $K_a = 0.059$, and with $R = 8.3145$ J K^{-1} mol^{-1}, and $T = 298$ K, we obtain $\Delta_r G_5 = 7.02$ kJ mol^{-1}.

References and Notes

(1) Legrand, M.; DeAngelis, M. *J. Geophys. Res.—Atmos.* **1996**, *101*, 4129.
(2) Smith, R.; Oremland, R. *Appl. Environ. Microb.* **1983**, *46*, 106.
(3) Edwards, M.; Benjamin, M. *J. Am. Waterworks Assoc.* **1992**, *84*, 56.
(4) Stern, M.; Heinzle, E.; Kut, O.; Hungerbuhler, K. *Water Sci. Technol.* **1997**, *35*, 329.
(5) Stockinger, H.; Heinzle, E.; Kut, O. *Enivron. Sci. Technol.* **1995**, *29*, 2016.
(6) Weavers, L.; Malmstadt, N.; Hoffmann, M. *Environ. Sci. Technol.* **2000**, *34*, 1280.
(7) Kotronarou, A.; Mills, G.; Hoffmann, M. *J. Phys. Chem.* **1991**, *95*, 3630.
(8) Liakou, S.; Kornaros, M.; Lyberatos, G. *Water Sci. Technol.* **1997**, *36*, 155.
(9) Vinodgopal, K.; Peller, J. *Res. Chem. Intermed.* **2003**, *29*, 307.
(10) Hara, K.; Osada, K.; Matsunaga, K.; Sakai, T.; Iwasaka, Y.; Furuya, K. *J. Geophys. Res.—Atmos.* **2002**, *107*, 4399.
(11) Stock, N.; Peller, J.; Vinodgopal, K.; Kamat, P. *Environ. Sci. Technol.* **2000**, *34*, 1747.
(12) Colarusso, P.; Serpone, N. *Res. Chem. Intermediat.* **1996**, *22*, 61.

(13) Bhandari, A.; Koul, S.; Sekhon, A.; Pramanik, S.; Chaturvedi, L.; Huang, M.; Menon, M.; Koul, H. *J. Urology* **2002**, *168*, 253.
(14) Miller, C.; Kennington, L.; Cooney, R.; Kohimoto, Y.; Cao, L.; Honeyman, T.; Pullman, J.; Jonassen, J.; Sceid, C. *Toxicol. Appl. Pharmacol.* **2000**, *162*, 132.
(15) Jonassen, J.; Cao, L.; Honeyman, T.; Scheid, C. *Crit. Rev. Euk. Gene Expr.* **2003**, *13*, 55.
(16) Allison, M.; Cook, H. *Science* **1981**, *212*, 675.
(17) Saffir, P.; Taube, H. *J. Am. Chem. Soc.* **1960**, *82*, 13.
(18) Jones, T.; Noyes, R. *J. Phys. Chem.* **1983**, *87*, 4686.
(19) Reckley, J.; Show Alter, K. *J. Am. Chem. Soc.* **1981**, *103*, 7012.
(20) Allen, T. *J. Am. Chem. Soc.* **1951**, *73*, 3589.
(21) Knoller, Y.; Perlmutter-Hayman, B. *J. Am. Chem. Soc.* **1955**, *77*, 3212.
(22) Domenech, J.; Peral, J. *J. Chem. Res.* **1987**, *11*, 360.
(23) Beltran, F.; Rivas, F.; Montero-de-Espinoza, R. *Ind. Eng. Chem. Res.* **2003**, *42*, 3210.
(24) Pines, D.; Reckhow, D. *Environ. Sci. Technol.* **2002**, *36*, 4046.
(25) Beltran, F.; Rivas, F.; Montero-de-Espinoza, R. *Ind. Eng. Chem. Res.* **2003**, *42*, 3218.
(26) Andreozzi, R.; Insola, A.; Caprio, V.; Marotta, R.; Tufano, V. *Appl. Catal., A* **1996**, *138*, 75.
(27) Andreozzi, R.; Caprio, V.; Insola, A.; Marotta, R.; Tufano, V. *Ind. Eng. Chem. Res.* **1997**, *36*, 4774.
(28) Draganic, Z.; Draganic, I.; Dosanic, M. *J. Phys. Chem.* **1964**, *68*, 2085.
(29) Draganic, Z.; Draganic, I.; Kosanic, M. *J. Phys. Chem.* **1966**, *70*, 1418.
(30) Getoff, N.; Schworer, F.; Markovic, V.; Sehested, K.; Nielsen, O. *J. Phys. Chem.* **1971**, *75*, 749.
(31) Peller, J.; Wiest, O.; Kamat, P. *J. Phys. Chem. A* **2001**, *105*, 3176.
(32) Naffrechoux, E.; Chanoux, S.; Petrier, C.; Suptil, J. *Ultrason. Sonochem.* **2000**, *7*, 255.
(33) Destaillats, H.; Colussi, A.; Joseph, J.; Hoffmann, M. *J. Phys. Chem. A* **2000**, *104*, 8930.
(34) Olson, T.; Barbier, P. *Water Res.* **1994**, *28*, 1383.
(35) Barbier, P.; Petrier, C. *J. Adv. Oxid. Technol.* **1996**, *1*, 154.
(36) Hung, H. M.; Hoffmann, M. R. *J. Phys. Chem.* **1999**, *103*, 2734.
(37) Smith, R.; Kilford, J. *Int. J. Chem. Kinet.* **1976**, *8*, 1.
(38) Curtis, A. R.; Sweetenham, W. P. *Facsimile/Checkmat Users Manual; Computer Science and Systems Division*, H. L., Ed.; United Kingdom Atomic Energy Authority: Oxford, England, 1987.
(39) Westerhoff, P.; Song, R.; Amy, G.; Minear, R. *Ozone-Sci. Eng.* **1997**, *19*, 55.
(40) Buxton, G.; Greenstock, C.; Helman, W.; Ross, A. *J. Phys. Chem. Ref. Data* **1988**, *17*, 513.
(41) Ross, A. B.; Mallard, W. G.; Helman, W. P.; Buxton, G. V.; Huie, R. E.; Neta, P. NDRL/NIST Solution Kinetics Data Base on the Web. In *NIST Standard Reference Database 40*; Notre Dame Radiation Laboratory and National Institute of Standards and Technology Notre Dame: Indiana and Gaithersburg, MD, 2002.
(42) Hua, I.; Hoffmann, M. *Environ. Sci. Technol.* **1997**, *31*, 2237.
(43) Hoigne, J.; Bader, H. *Water Res.* **1983**, *17*, 185.
(44) Weavers, L. K.; Hoffmann, M. R. *Environ. Sci. Technol.* **1998**, *32*, 3941.
(45) Didenko, Y. T.; McNamara, W. B.; Suslick, K. S. *J. Phys. Chem. A* **1999**, *103*, 10783.
(46) Didenko, Y. T.; McNamara, W. B.; Suslick, K. S. *J. Am. Chem. Soc.* **1999**, *121*, 5817.
(47) Flannigan, D. J.; Suslick, K. S. *Nature* **2005**, *434*, 52.
(48) Suslick, K. S.; Flannigan, D. J. *Annu. Rev. Phys. Chem.* **2008**, *59*, 659.
(49) Elliot, A.; Buxton, G. *J. Chem. Soc. Faraday T.* **1992**, *88*, 2465.
(50) Bielski, B.; Cabelli, D.; Arudi, R.; Ross, A. *J. Phys. Chem. Ref. Data* **1985**, *14*, 1041.
(51) Mason, T.; Lorimer, J. *Applied Sonochemistry. The Uses of Power Ultrasound in Chemistry and Processing*; Wiley-VCH: Weinheim, Germany, 2002.
(52) Flyunt, R.; Schuchmann, M.; von Sonntag, C. *Chem.—Eur. J.* **2001**, *7*, 796.
(53) Fojtik, A.; Czapski, G.; Henglein, J. *J. Phys. Chem.* **1970**, *74*, 3204.
(54) Buxton, G. V.; Sellers, R. M. *J. Chem. Soc. - Faraday Trans. I* **1973**, *69*, 555.
(55) Jeevarajan, A. S.; Carmichael, I.; Fessenden, R. W. *J. Phys. Chem.* **1990**, *94*, 1372.
(56) Surdhar, P. S.; Mezyk, S. P.; Armstrong, D. A. *J. Phys. Chem.* **1989**, *93*, 3360.
(57) Hart, E.; Henglein, A. *J. Phys. Chem.* **1985**, *89*, 4342.
(58) Staehelin, J.; Hoigne, J. *Environ. Sci. Technol.* **1982**, *16*, 676.
(59) Bielski, B.; Richter, H. W. *J. Am. Chem. Soc.* **1977**, *99*, 3019.
(60) Beckett, M.; Hua, I. *Environ. Sci. Technol.* **2000**, *34*, 3944.
(61) Joseph, J.; Destaillats, H.; Hung, H.; Hoffmann, M. *J. Phys. Chem. A* **2000**, *104*, 301.
(62) Destaillats, H.; Lesko, T.; Knowlton, M.; Wallace, H; Hoffmann, M. *Ind. Eng. Chem. Res.* **2001**, *40*, 3855.
(63) Bennett, L.; Warlop, P. *Inorg. Chem.* **1990**, *29*, 1975.
(64) Schwarz, H.; Dodson, R. *J. Phys. Chem.* **1984**, *88*, 3643.
(65) Klaning, U.; Sehested, K.; Holcman, J. *J. Phys. Chem.* **1985**, *89*, 5271.
(66) Staehelin, J.; Hoigne, J. *Environ. Sci. Technol.* **1979**, *16*, 676.
(67) Gottschalk, C.; Libra, J.; Saupe, A. *Ozonation of Water and Waste Water. A Practical Guide to Understanding Ozone and its Application*; Wiley-VCH: New York, 2000.
(68) Weavers, L.; Ling, F.; Hoffmann, M. *Environ. Sci. Technol.* **1998**, *18*, 2727.
(69) Hart, E.; Henglein, A. *J. Phys. Chem.* **1986**, *90*, 3061.
(70) Kang, J.; Hung, H.; Lin, A.; Hoffmann, M. *Environ. Sci. Technol.* **1999**, *33*, 3199.
(71) Colussi, A.; Hoffmann, M. *J. Phys. Chem. A* **1999**, *103*, 2696.
(72) Sehested, K.; Holcman, J.; Bjergbakke, E.; Hart, E. *J. Phys. Chem.* **1984**, *88*, 4144.
(73) Brunet, R.; Bourbigot, M.; Dore, M. *Ozone Sci. Eng.* **1984**, *6*, 163.
(74) Kang, J.; Hoffmann, M. *Environ. Sci. Technol.* **1998**, *32*, 3194.
(75) Acero, J.; Von Gunten, U. *J. Am Water Works Assoc.* **2001**, 90.
(76) Elovitz, M.; von Gunten, U. *Ozone Sci. Eng.* **1999**, *21*, 239.
(77) Elovitz, M.; von Gunten, U.; Kaiser, H. *Ozone Sci. Eng.* **2000**, *22*, 123.
(78) Paillard, H.; Brunet, R.; Dore, M. *Water Res.* **1988**, *22*, 91.
(79) Petrier, C.; Francony, A. *Ultrason. Sonochem.* **1997**, *4*, 295.
(80) Lesko, T. M.; Colussi, A. J.; Hoffmann, M. R. *J. Am. Chem. Soc.* **2004**, *126*, 4432.
(81) Wentworth, P.; Wentworth, A.; Zhu, X.; Wilson, I.; Janda, K.; Eschenmoser, A.; Lerner, R. *Proc. Natl. Acad. Sci.* **2003**, *100*, 1490.
(82) Xu, X.; Goddard, G. I. *Proc. Natl. Acad. Sci.* **2002**, *99*, 15308.
(83) Christensen, H.; Sehested, K.; Corfitzen, H. *J. Phys. Chem.* **1982**, *86*, 1588.
(84) Lind, J.; Merenyi, G.; Hohansson, E.; Brink, T. *J. Phys. Chem.* **2003**, *107*, 676.
(85) Atkins, P. *Physical Chemistry*, 5 ed.; W. H. Freeman and Company: New York, 1994.
(86) Colussi, A. J. In *Chemical Kinetics of Small Organic Radicals*; Alfassi., Z., Ed.; CRC Press: Boca Raton, Fl, 1988; Vol 1; pp 150.
(87) Benson, S. *Thermochemical Kinetics*, 2 ed.; Wiley: New York, 1976.
(88) Lesko, T.; Colussi, A. J.; Hoffmann, M. R. *Environ. Sci. Technol.* **2006**, *40*, 6818.

JP9115386